Inorganic Chemistry

Article

pubs.acs.org/IC

Spectroscopic and Magnetic Properties of the Metastable States in the Coordination Network $[\{Co(prm)_2\}_2\{Co(H_2O)_2\}\{W(CN)_8\}_2]\cdot 4H_2O$ (prm = pyrimidine)

Rémy Le Bris,[†,‡] Yoshihide Tsunobuchi,[§] Corine Mathonière,*[,†,‡] Hiroko Tokoro,[§] Shin-ichi Ohkoshi,[§] Nawel Ould-Moussa,[⊥] Gabor Molnar,[⊥] Azzedine Bousseksou,[⊥] and Jean-François Létard.[†,‡]

[†]CNRS, ICMCB, UPR 9048, F-33600 Pessac, France

[‡]Univ. Bordeaux, ICMCB, UPR 9048, F-33600 Pessac, France

[§]Department of Chemistry, School of Science, The University of Tokyo, 7-3-1 Hongo, Bunkyo-ku, Tokyo 113-0033, Japan

[⊥]Laboratoire de Chimie de Coordination, CNRS, UPR 8241, Université de Toulouse (UPS, INP) 205, Route de Narbonne, 31077 Toulouse, France

Supporting Information

ABSTRACT: The study of the metastable states, obtained by thermal quenching or by light irradiation in the $[\{Co(prm)_2\}_2\{Co(H_2O)_2\}\{W(CN)_8\}_2]\cdot 4H_2O$ complex, is reported using powder X-ray diffraction, Raman spectroscopy, optical reflectivity, and magnetic measurements. This compound is characterized by a electron-transfer (ET) phase transition occurring between a high-temperature phase (HT phase) formed by paramagnetic $Co^{II}-W^{V}$ units and a low-temperature phase (LT phase) formed by diamagnetic $Co^{III}-W^{IV}$ units. Metastable phases can be induced at low temperature either by thermal quenching rapidly cooling phase named RC or by irradiation photo-induced phase named PI similar to the well-known Light-Induced Excited Spin State Trapping effect. The relaxation dynamics of the metastable phases have been studied and revealed some differences between the RC and PI phases. The sigmoidal shape of the relaxation curves in the RC phase is in agreement with the cooperative nature of the process. Thermodynamic parameters that govern the relaxation have been determined and used to reproduce the experimental Thermal-Induced Excited Spin State Trapping curve.

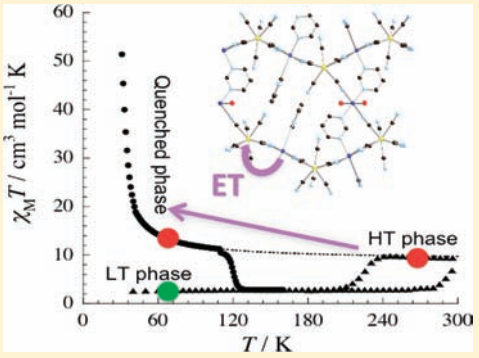

INTRODUCTION

The cyano-bridged coordination compounds are very fascinating materials because they exhibit a large variety of useful chemical properties, such as molecular sieves[1] and medical treatment[2] or hydrogen-storage materials,[3] and also physical properties, such as magnetism.[4] Some of these systems present switchable properties, with the switching being induced by an external stimulus such as current,[5] pressure,[6] electric field,[7] and light or temperature.[8] These functionalities open interesting perspectives in data storage. For instance, the nonstoichiometric networks, the well-known Prussian Blue analogues, built from the anionic $[Fe^{II}(CN)_6]^{4-}$ complex and Co^{3+} cations behave as photomagnets with optical control of the Curie temperature.[9] This phenomenon is caused by a light-induced charge transfer in the diamagnetic $Fe^{II}-CN-Co^{III}$ pairs, giving rise to paramagnetic $Fe^{III}-CN-Co^{II}$ pairs. The properties of these networks formulated as $Cat_xCo[Fe(CN)_6]_y\cdot zH_2O$ with $y < 1$ have been optimized with chemical control of the amount of $[Fe(CN)_6]$ vacancies filled by water molecules. The photomagnetic properties of these networks have been studied in detail by several groups.[10] It has been shown that charge transfer can be thermally induced and light-induced in a reversible manner. Moreover, it turns out that, based on powder X-ray structural and spectroscopic studies, only the compounds with a mean environment of Co with five N atoms (from CN bridges) and one O atom (from H_2O molecules filling the vacancies) are photomagnetically active. Using transient absorption spectroscopy, it has been shown also that the change of the properties under light irradiation is not only due to a charge transfer between metal centers but also to a spin change centered on the Co ion,[11] accompanied by an important variation of Co−N bond lengths.[12] Ohkoshi et al. have called this phenomenon a "charge-transfer-induced spin transition" (CTIST), emphasizing the strong analogy of the charge-transfer phenomenon with the photoinduced spin transition in molecular complexes.[13] Recently, this family of photomagnetic Prussian Blue analogues was enriched with several structurally characterized cyanide-bridged iron/cobalt molecular compounds that mimic the electronic properties of the 3D networks at the molecular scale.[14−17]

Received: September 7, 2011
Published: February 22, 2012

 © 2012 American Chemical Society dx.doi.org/10.1021/ic2019692 | *Inorg. Chem.* 2012, 51, 2852−2859

Other systems prepared with 5d cyanometalates, $[Os^{III/II}(CN)_6]^{3-/4-}$,[18] and $[W^{IV/V}(CN)_8]^{4-/3-}$,[19,20] and with Co ions have been described to show CTIST phenomena between the Os (or W) and Co ions. They have also been structurally characterized, and both present extended networks: one cubic structure with $\{Os^{III}(CN)_6\}$ similar to the Fe/Co Prussian Blue analogues and two less symmetrical structures with the octacyanometalates $\{W^{V}(CN)_8\}$. The first compound, $Cs[\{Co(3\text{-cyanopyridine})_2\}\{W(CN)_8\}]\cdot H_2O$, is a 2D network and the second one, $[\{Co(prm)_2\}_2\{Co(H_2O)_2\}\{W(CN)_8\}_2]\cdot 4H_2O$, is a 3D network. The architecture of these two compounds shows some analogies, with a layered structure of W and Co linked by four cyano groups and two organic ligands between the layers completing the coordination sphere of the Co ion. As 3-cyanopyridine acts as a separator for the layers for the 2D compound, the pyrimidine (prm) ligand is connecting the layers, forming a 3D network in the late compound.

Recently, we described the metastable phase generated at low temperature by light irradiation in the 2D network using optical and magnetic properties.[19b] We have also observed that it was possible to reach a metastable phase by rapid cooling. We have carefully studied the relaxation processes using magnetic techniques and then determined the thermodynamical parameters governing the dynamics and lifetimes of the metastable states. These parameters are crucial for the use of such kinds of materials in devices, but they remain very rarely determined in charge-transfer complexes. A part of our current work is to select some representative examples of charge-transfer compounds to determine the relaxation dynamics using the same methodology as that used for the light-induced spin crossover.[21,22]

In the present work, we are interested in a detailed description of the metastable states of the photomagnetic compound $[\{Co(prm)_2\}_2\{Co(H_2O)_2\}\{W(CN)_8\}_2]\cdot 4H_2O$. These metastable states are generated by light irradiation and, for the first time, by rapid cooling. In this study, our objective is to compare these two metastable states through their detailed description using powder X-ray diffraction (XRD), magnetometry, and Raman and optical spectroscopies. Then, we carefully investigate the relaxation of the magnetic metastable quenched phase by recording the kinetics as a function of time. Finally, we simulate the thermal dependence of the magnetic properties in the thermally quenched phase at a warming rate of 0.3 $K\cdot min^{-1}$.

EXPERIMENTAL SECTION

Synthesis of Complex $[\{Co(prm)_2\}_2\{Co(H_2O)_2\}\{W(CN)_8\}_2]\cdot 4H_2O$ (1). Compound **1** was prepared according to the literature.[20] An aqueous solution (2.5 mL) of $Cs^{I}_3[W^{V}(CN)_8]\cdot 2H_2O$[21] (0.12 M) was added to a mixed aqueous solution (2.5 mL) of $Co^{II}Cl_2\cdot 6H_2O$ (0.19 M) and pyrimidine (prm; 0.25 M) at room temperature. The red precipitated powder was filtered, washed with water, and allowed to dry in air. Elemental analysis confirmed that the formula was $[\{Co(prm)_2\}_2\{Co(H_2O)_2\}\{W(CN)_8\}_2]\cdot 4H_2O$. Calcd: Co, 12.72; W, 26.47; C, 27.67; H, 2.03; N, 24.2. Found: Co, 12.65; W, 26.81; C, 27.76; H, 2.00; N, 24.50.

Powder XRD. The powder XRD patterns were measured by a Rigaku RINT2100 with Cu Kα (λ = 1.5406 Å) at 293 K. Rietveld analyses were performed by the *PDXL* program (Rigaku).[23]

Raman Studies. Raman spectra were collected using a LabramHR (Jobin-Yvon) Raman spectrometer equipped with an Olympus BXFM microscope using a 1800 mm^{-1} grating, a 100 μm spectrograph slit, and an Andor Technology 1024 × 256 format charge-coupled-device (CCD) detector (pixel size 26 μm); a spectral resolution of ca. 1 cm^{-1} was achieved. The excitation laser light (632.8 nm, 10 μW) was focused on the sample by a long-working-distance, 50× objective (numerical aperture = 0.5). The temperature of the sample was controlled using a Linkam THMS600 liquid-nitrogen cryostat. Taking into account the sample nature (fine microcrystalline powder), polarization studies were not carried out.

Optical Reflectivity Studies. The optical properties were investigated using a home-built reflectivity system equipped with a CVI spectrometer, which allows us, first, to collect reflectivity spectra, within the range of 500−900 nm, at different temperatures and, second, to observe the temperature dependence of the signal at two different wavelengths (±2.5 nm) between 10 and 290 K. The scanning rate in temperature is 3 $K\cdot min^{-1}$. Experiments were performed on a thin layer of powder.

Magnetic and Photomagnetic Measurements. The magnetic properties were investigated with a MPMS-5S Quantum Design SQUID (Superconducting Quantum Interference Device) magnetometer operating with an external magnetic field of 0.5 T within the range of 5−350 K. The measurements were performed on a sample of 10.9 mg placed in a gelatin cap. For thermal quenching (or rapid cooling), the sample was first warmed at 350 K in the SQUID cavity, and then the sample was removed from the SQUID introducing chamber before it was reloaded into the SQUID cavity, frozen at 30 K, in a few seconds. The experimental data were corrected for the diamagnetic contribution by using Pascal's constants.[24,25] The photomagnetic properties were performed using a Spectrum Physics Beamlok 2060 laser (λ = 647 nm) coupled via an optical fiber to the cavity of a MPMS-5S Quantum Design SQUID magnetometer. Samples consisted of a thin layer of compound whose weight was obtained by a comparison of the curve with a more accurately weighed sample of the same material. The sample was irradiated (λ = 647 nm) at T = 30 K during more than 15 h. The optical power at the sample surface was adjusted to 5 $mW\cdot cm^{-2}$, in order to minimize the heating of the sample. The Thermal-Induced Excited Spin State Trapping (TIESST) and Light-Induced Excited Spin State Trapping (LIESST) curves were measured by following the previously published methods described for iron(II) spin-crossover materials.[21] It consists of warming the sample at a rate of 0.3 $K\cdot min^{-1}$ and recording the magnetization at each Kelvin interval. The T(TIESST) and T(LIESST) temperatures were then extracted from the minimum of the $d\chi_M T/dT$ vs T plots.

According to previous results published for spin-crossover compounds[21] and for the 2D octacyanotungstate network,[19] the magnetic behavior versus temperature of the RC phase was simulated using the master equation (1):

$$\left(\frac{\partial \gamma_{RC}}{\partial t}\right)_{Ti} = -\gamma_{RC}[k_{HL}(T \to 0) + k_{HL}(T \to \infty)\, e^{-E_a/k_B T_i} e^{\alpha(T_i)(1-\gamma_{RC})}] \quad (1)$$

where γ_{RC} is the RC phase (which is the rapidly cooled, i.e., thermally quenched, phase) fraction, $k_{HL}(T\to 0)$ is the estimated rate constant in the quantum tunnelling region, $k_{HL}(T\to\infty)$ is the rate constant in the thermally activated region, E_a is the activation energy, and α is the self-acceleration factor. For the simulations performed using software *Maple10*, we used an analytical expression, $(\chi_M T)_{mag}$,[26] with parameters obtained with the Curie−Weiss fit of the $1/\chi_M$ vs T plot for a ferromagnetic material above its Curie temperature. The resulting $(\chi_M T)_{mag}$ curve corresponds to a hypothetical high-temperature phase (HT phase) in the entire temperature range. The simulation of the TIESST curve is then expressed following equation (2):

$$\chi_M T_i = (\chi_M T)_{mag}\gamma_{RC}(t, T_i) \quad (2)$$

RESULTS AND DISCUSSION

Synthesis and Structure. The compound has been prepared in its powder form, as reported in the literature. Using powder XRD (Figure 1a), the material exhibits at room

dx.doi.org/10.1021/ic2019692 | *Inorg. Chem.* 2012, 51, 2852−2859

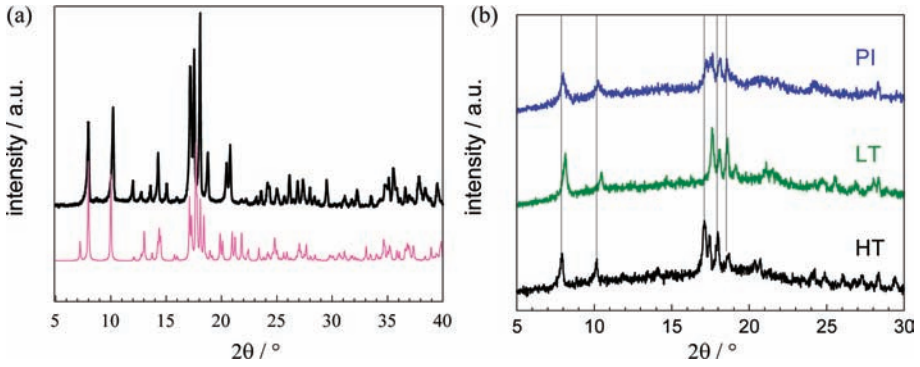

Figure 1. (a) Comparison between the experimental XRD pattern (black line) for compound **1** and the simulated XRD pattern for the crystal X-ray study (pink line).[20b] (b) Experimental XRD patterns at 298 K (black line), at 20 K (green line, LT for low temperature), and at 20 K after red-light irradiation (blue line, PI for the photoinduced phase).

temperature a monoclinic symmetry with the space group $P2_1/n$ with a = 7.596(4) Å, b = 13.903(7) Å, c = 22.245(12) Å, and β = 95.813(8)°. These cell parameters are in agreement with those recently published.[20] Then, **1** is a 3D network formed by grids in ab planes composed of W−CN−Co1 arrays, with these layers being connected along the c direction by Co2 ions, prm molecules, and cyanide bonds. At 20 K, the powder XRD pattern presents the same peaks but shifted (Figure 1b). In the low-temperature phase (LT phase), the space group $P2_1/n$ is preserved, but the cell parameters are different: a = 7.3534(14) Å, b = 13.359(2) Å, c = 21.672(4) Å, and β = 95.231(15)°. To check the photosensitivity of **1**, the powder has been irradiated with red light for 20 min (750 nm, 60 mW·cm^{-2}, 14 K). The resulting photoinduced XRD pattern (Figure 1b) is similar than the XRD pattern of the HT phase. This shows clearly that the photoinduced phase formed in this experiment is similar to the HT phase, but contains also a residual LT phase, which suggests an incomplete photo-transformation.

Magnetic Properties. We checked the occurrence of the thermal transition in the new prepared sample (Figure 2). The

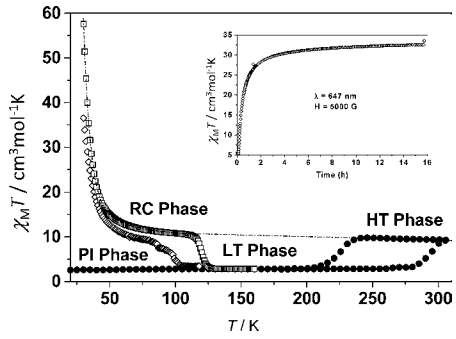

Figure 2. Magnetic measurements performed at 0.5 T on **1**: (●) thermal transition (sweeping rate: 2 K·min^{-1}) between the HT and LT phases; (□) rapid-cooled (RC) phase obtained after thermal quench (sweeping rate: 0.3 K·min^{-1}) ; (◇) photo-induced (PI) phase obtained after red-light irradiation from the LT phase (sweeping rate: 0.3 K·min^{-1}). In insert: time dependence at 10 K of the χT product during red-light irradiation.

magnetic properties obtained in the dark are plotted as the thermal dependence of the product of the molar magnetic susceptibility (χ_M defined as M/H) and the temperature T (Figure 2). In agreement with the previously reported results,[20] a temperature-induced phase transition between the HT and LT phases is observed with a wide thermal hysteresis loop with $T_{1/2}(\downarrow)$ = 225 K and $T_{1/2}(\uparrow)$ = 295 K. The $\chi_M T$ product at 310 K is equal to 9.34 cm^3·K·mol^{-1} and corresponds to the HT phase with two W^V metal ions ($S = {}^1/_2$; g = 2) and three Co^{II} metal ions in a high spin state ($S = {}^3/_2$; g = 2.47). Below 190 K, the $\chi_M T$ product is equal to 2.80 cm^3·K·mol^{-1}, which is in agreement with only one Co^{II} metal ion in a high spin state ($S = {}^3/_2$; g = 2.45).

Raman Spectroscopic Properties: Thermal- and Light-Induced Properties. As reported before,[7] the LT and HT phases of **1** have been identified by Raman spectra in the CN stretching modes region around 2200 cm^{-1} in the thermal hysteresis loop (at 250 K). Here, we have followed the electron-transfer transition by measuring the Raman spectra in the 2100−2300 cm^{-1} region at room temperature and at 140 K (Figure 3). The observed Raman changes are also associated

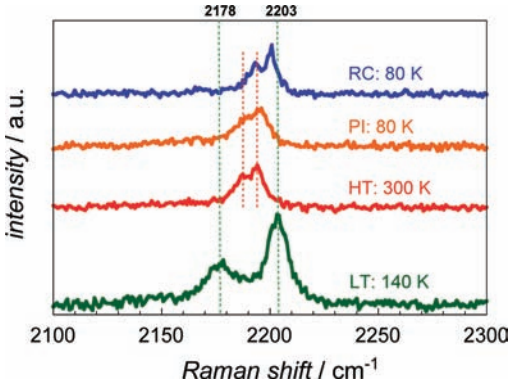

Figure 3. Raman spectra recorded in the cyanide region for **1** (2100−2300 cm^{-1}) in the dark (bottom) at 140 K (LT phase, green) and at 300 K (HT phase, red). (top) Raman spectra of the metastable phases at 80 K generated by light irradiation (PI phase, orange) or by rapid cooling (RC phase, blue). The dashed lines are eye guides to indicate in green the peaks in the LT phase and in red the peaks in the HT phase.

with a color change during cooling from a red color at room temperature to a blue color at 140 K (Figure S1 in the Supporting Information). The spectrum at room temperature is typical of the HT phase with the presence of two close peaks (2194 and 2187 cm^{-1}).[7] After cooling at 140 K, the spectrum shows also two well-defined peaks (2203 and 2178 cm^{-1}) and is similar to the spectrum attributed previously to the LT phase.[7] The attribution of the two modes in each phase is not straightforward for two reasons: (i) both phases contain several

dx.doi.org/10.1021/ic2019692 | Inorg. Chem. 2012, 51, 2852−2859

types of CN bridges (nonbridging and $W^{V}-CN-Co^{II}$ for the HT phase; nonbridging, $W^{IV}-CN-Co^{III}$, and $W^{IV}-CN-Co^{II}$ for the LT phase), and (ii) no data are available in the literature for these pairs. The energies of these Raman modes are comparable with the IR spectra of the LT and HT phases in **1**.[20] In the course of our study, we have also investigated by Raman spectroscopy the parent 2D network $Cs[\{Co(3\text{-cyanopyridine})_2\}\{W(CN)_8\}]\cdot H_2O$, which presents a electron-transfer transition between a $Co^{II}W^{V}$ HT phase and a $Co^{III}W^{IV}$ LT phase. The Raman spectra of the 2D network are shown in Figure S2 in the Supporting Information in its HT (300 K) and LT (120 K) phases. As for **1**, the two phases of the 2D network present peaks for cyanide bridges that are close in energy for the HT phase and more separated in the LT phase. This seems, therefore, to be a characteristic Raman feature differentiating the $W^{V}-CN-Co^{II}$ and $W^{IV}-CN-Co^{III}$ pairs.

The existence of the metastable states for **1** has been investigated by a Raman technique either by (i) light irradiation at 80 K or by (ii) a rapid cooling from 300 K. Figure 3 shows a comparison between the three spectra recorded at room temperature (HT phase), after light irradiation (PI phase), and after thermal quenching (RC phase) at 80 K. All present a similar two-peak structure shape. The energy difference between the two peaks remains identical for the three spectra (around 7 cm^{-1}). This suggests that the PI and RC phases are similar to the HT phase. The energy shift observed between the spectra in the HT phase (300 K) and those in the PI and RC phases (recorded at 80 K) is probably attributed to a thermal effect. This Raman study clearly shows that the spectroscopic properties of the quenched (RC) and photoinduced (PI) phases are close to those of the HT phase.

Diffuse Reflectivity Properties. To probe the color changes during the transition, we investigated optical spectra of the compound using the reflectivity technique when the compound is upon constant white-light irradiation. Figure 4

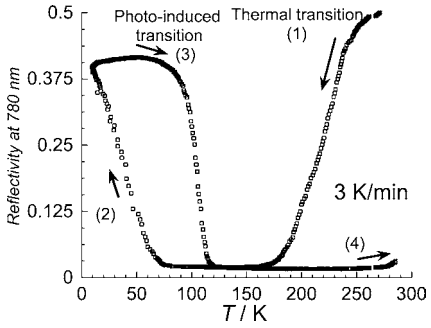

Figure 4. Thermal dependence of the light intensity reflected by **1** at wavelength $\lambda = 780 \pm 5$ nm during cooling (1 and 2) and warming (3 and 4) modes (3 $K\cdot min^{-1}$).

presents the thermal variation of the reflected light intensity by the sample at the specific wavelength 780 ± 5 nm. Upon cooling, the reflectance at 780 nm shows a first decrease (1) from 0.5 at 280 K to 0.02 at 150 K. This value remains almost constant until 80 K, and then the signal increases (2) to reach 0.4 at 10 K. Upon warming from 10 K, no change in the reflected intensity is observed up to 80 K. Above this temperature, the signal decreases (3) to reach the previously observed value 0.02 at 150 K. No more specific changes are observed up to 280 K. These thermal variations of the optical properties have already been observed for spin-crossover[27] and charge-transfer compounds.[10] They are attributed to a temperature-induced transition (1) between the HT and LT phases and to a light-induced transition (2). Actually, this study confirms that at low temperatures a metastable photoinduced phase (PI phase) is formed. The cooling and heating modes (3 $K\cdot min^{-1}$) give rise to two hysteresis loops: one well-defined at low temperatures corresponding to light-induced thermal hysteresis[28] and another one at higher temperatures corresponding to thermal-induced hysteresis. Note that this second hysteresis loop is not closed at 280 K, which is the final temperature in our reflectivity setup, but is expected to be complete at 300 K, in agreement with the magnetic results. The observation of these loops confirmed the magnetic results and reflects the cooperativity existing in this 3D network.

To fully understand these optical changes, it is interesting to study the absorption spectra at different temperatures. Figure 5 presents the thermal dependence of the absorption spectra during cooling from 280 to 10 K. In the HT phase, at 240 K the spectrum shows a broad band below 750 nm, with a maximum at 550 nm, which has been previously attributed to a metal–metal charge-transfer (MMCT) band $Co^{2+} \rightarrow W^{5+}$.[20] Upon cooling, this band is decreasing in intensity, whereas a new band, centered around 760 nm, is increasing gradually down to 150 K. This new band can be attributed to the MMCT band $W^{4+} \rightarrow Co^{3+}$.[20] These thermal changes of the spectra correspond to the thermal transition already observed in the magnetic measurements in the 300–150 K range. Similar changes, but in opposite ways, are observed from 150 to 10 K. Because the spectrum at 10 K is very close to the one recorded at 240 K, the resulting PI phase has a spectrum close to that of the HT phase. Along these spectral (thermal- and light-induced) changes, two isosbestic points are observed. During the thermal transition (300–150 K), one is observed at 594 nm whereas during photoinduced transition (below 150 K) the other one appears at 607 nm. The existence of these isosbestic points indicates that during the thermal- and light-induced processes the same independent phases are involved and changed in magnitude. The slight energy difference between the two isosbestic points may be attributed to the temperature dependence of the parameters governing the two transitions.

Photomagnetic Properties. Then, the photomagnetic properties of **1** have been investigated. The inset in Figure 2 presents the formation of the photoinduced phase. At 30 K, the $\chi_M T$ product increased upon light excitation (λ = 647 nm) and reached a saturation value of 37 $cm^3\cdot mol^{-1}\cdot K$ after 16 h. When the light is switched off, the magnetic characterization of the photoproduct is started with a temperature increase of 0.3 $K\cdot min^{-1}$. Figure 2 shows the magnetic responses of the photoinduced phase (PI phase) and also of the thermally quenched phase (obtained after a rapid cooling at 30 K, phase noted RC phase). The two phases present similar magnetic behaviors. When the temperature is increased from 30 K, a rapid decrease of the $\chi_M T$ product is first observed from 57.60 $cm^3\cdot K\cdot mol^{-1}$ at 30 K to 11.44 $cm^3\cdot K\cdot mol^{-1}$ at 80 K for the RC phase and from 36.52 $cm^3\cdot K\cdot mol^{-1}$ at 30 K to 9.26 $cm^3\cdot K\cdot mol^{-1}$ at 80 K for the PI phase. This can be assigned to the ferromagnetic interactions between Co^{2+} and W^{5+}.[20] When the temperature is increased further, the magnetic signals become more or less constant, in the range 80–110 K for the RC phase with a value of around 10.80 $cm^3\cdot K\cdot mol^{-1}$ and in the range 80–90 K for the PI phase with a value of around 8.30 $cm^3\cdot K\cdot mol^{-1}$. Finally, the magnetic signal decreases rapidly to recover the representative $\chi_M T$ value of the LT phase (2.80

dx.doi.org/10.1021/ic2019692 | Inorg. Chem. 2012, 51, 2852–2859

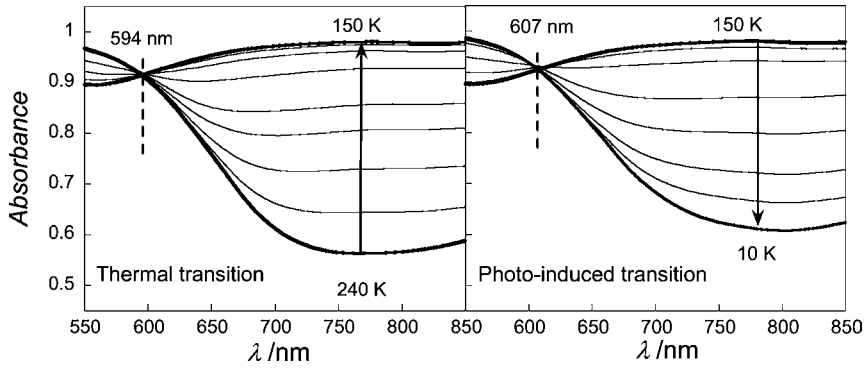

Figure 5. Absorption spectra recorded at the surface of **1** during cooling from 240 to 150 K (left picture) and from 150 to 10 K (right picture).

$cm^3 \cdot K \cdot mol^{-1}$) at around 130 K for the RC phase and 110 K for the PI phase. These curves allow the determination of TIESST = 120 K for the RC phase and T(LIESST) = 98 K for the PI phase, as the extrema of $d\chi_M T/dT$ vs T. From that, it is suggested that the decay process is faster in the PI phase than in the RC phase. Moreover, the $\chi_M T$ values in the PI phase are lower than those in the RC phase in the entire temperature range. As shown by the fit curve of the HT phase in Figure 2, the $\chi_M T$ values in the RC phase are close to the values that we expect for the Co^{II}–W^V phase. This shows that in the RC phase all of the Co^{II}–W^V pairs are quantitatively trapped. On the contrary, photoconversion in the PI phase appears lower, with reminescence of some Co^{III}–W^{IV} pairs in the material. This type of difference may be attributed to the deep color of the sample, which may prevent light penetration. Along those lines, the absorption spectrum of the LT phase (Figure 5, 150 K) is much more absorbing in comparison with the one recorded in the HT phase at 240 K. Consequently, during irradiation, this 3D compound can be viewed as a biphased material, with the first top layers of the sample completely transformed and the bottom ones almost unexcited, leading to intermediate $\chi_M T$ values between the ones of the LT and RC phases at a fixed temperature. This partial photoconversion has already been seen in **1** with XRD patterns of the PI phase (see Figure 1b) and also in our previous study of the parent Co–W 2D network.[19] However, compared to the 2D network, where T(LIESST) = 115 K and T(TIESST) = 117 K have been found to be similar, the Co–W 3D network presents significant differences between these two temperatures, suggesting some differences in the PI and RC phases. Interestingly, differences between the PI and RC phases have also been reported in a photomagnetic Co–Fe$(CN)_6$ compound,[29] and synchroton X-ray measurements showed small local structural differences, with a local and disordered tilting of the polyhedra of Fe$(CN)_6$ between the RC and PI phases. Our results indicate also that the PI phase formed at low temperature showed small structural differences/deformations compared to the HT phase. This observation is also coherent with the reflectivity measurements with the presence of two isosbestic points in the PI and RC phases, respectively.

Relaxation Kinetics. Because the RC phase is quantitatively trapped, we investigated further its thermal relaxation. For that, we have carried out relaxation kinetics using magnetometry from 90 to 118 K. Figure 6 shows the time dependence of the RC fraction, γ_{RC}, as a function of the temperature. The γ_{RC} fraction, as indicated in the Experimental Section, was deduced from the $[(\chi_M T) - (\chi_M T)_{LT}]/[(\chi_M T)_{mag} - (\chi_M T)_{LT}]$ ratio, where $(\chi_M T)_{mag}$ represents the temperature

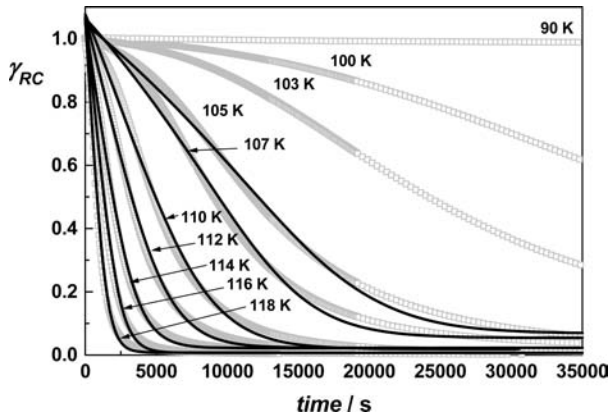

Figure 6. Relaxation kinetics of the RC phase recorded at different temperatures. Lines correspond to fits with a sigmoidal decrease.

dependence of the magnetic properties of the material remaining in the HT phase in the entire temperature range (2–300 K; see Figure 2). Below 90 K, the relaxation is nearly temperature independent. For instance, at 90 K the relaxation process represents less than 1.5% after 7 h. This observation suggests that the relaxation process is governed below 90 K by the quantum tunnelling regime.[30] In this regime, the determination of the relaxation rate $k_{HL}(T \rightarrow 0)$ remains difficult because of the long lifetime of the RC phase at these temperatures. That is the reason why we only estimate an upper limit of $k_{HL}(T \rightarrow 0)$ with the relaxation rate of the fitted curve at the lowest temperature. For this compound, the relaxation rate is estimated at 105 K and $k_{HL}(T \rightarrow 0) < 3.57 \times 10^{-5}$ s^{-1} (Table 1). Between 100 and 118 K, the relaxation

Table 1. Relaxation Rates and α Factor Extracted at Each Temperature from the Fitting of the Relaxation Curves

T (K)	τ (s)	k_{HL} ($\times 10^{-5}$ s^{-1})	α	E_a* (cm^{-1})
105	28010	3.57	2	145.8
107	20000	5	1.96	145.6
110	8620	11.6	1.27	97.0
112	5620	17.8	1.2	93.3
114	3390	29.5	1.1	87.1
116	2320	43.1	1.15	92.6
118	1390	71.9	0.98	80.3

process is thermally activated, and the kinetic curves show a clear deviation from a single-exponential decay. The relaxations show a sigmoidal shape (slow initial decay followed by a faster relaxation and finally a slowing down). This behavior is

dx.doi.org/10.1021/ic2019692 | Inorg. Chem. 2012, 51, 2852–2859

consistent with a self-accelerated behavior predicted for strong cooperative systems.[10,22,31] The relaxations can be modeled using the mean-field approach with Hauser's model, based on Buhks theory,[30] which has been originally reported for spin-crossover materials, where the internal pressure arises from the large difference in metal−ligand bond lengths between high-spin and low-spin states. This model has been also used for charge-transfer materials.[10d,19b] In this model, the relaxation rate $k_{HL}(T, \gamma_{RC})$ depends exponentially on both γ_{RC} and T (eqs 3 and 4) and the self-accelerating parameter $\alpha(T)$ at a given temperature, which represents the cooperativity of the system.

$$\frac{d\gamma_{RC}}{dt} = -k_{HL}(T, \gamma_{RC})\,\gamma_{RC} \quad (3)$$

$$k_{HL}(T, \gamma_{RC}) = k_{HL}(T)\, e^{\alpha(T)(1-\gamma_{RC})} \quad (4)$$

with

$$k_{HL}(T) = k_{HL}(T \to \infty)\, e^{-E_a/k_BT}\ \alpha(T) = \frac{-E_a^*}{k_BT}$$

On the basis of this sigmoidal treatment, the relaxation curves can be satisfactorally fitted (solid lines in Figure 6), and the deduced parameters are reported in Table 1. An average value of the additional energy E_a* linked to the cooperativity is then estimated at 106 cm^{-1}.

The occurrence of a self-accelerated behavior is consistent with the cooperativity reflected by the wide thermal hysteresis loop (225−295 K, ΔT = 70 K). Self-acceleration can be attributed to contraction of the Co site between the RC and LT phases, as shown experimentally with a decrease of the Co−N bond lengths of around 0.2 Å in FeCo Prussian Blue analogues[12] and molecular compounds[16,17] and also in the parent Co−W 2D network.[32] This decrease at the atomic level has important effects on the relaxation curves with slow formation of the first contracted Co sites followed by an accelerated propagation of the phenomenon. The relaxation curves have been well reproduced with the Hauser model, where self-acceleration is explained by an internal pressure in the lattice and a progressive lowering of the energy barrier between the different states.

The Arrhenius plot of $\ln[k_{HL}(T)]$ vs $1/T$ is shown in Figure 7. A linear fit allows one to determine the activation energy E_a = 2010 cm^{-1} and frequency factor $k_{HL}(T\to\infty)$ = 3.13 × 10^7 s^{-1} for the RC phase. These parameters enable us to estimate the lifetimes of the RC state at any temperature using the relation $\tau = 1/k_{HL}(T)$. For example, at 170 K, the lifetime is estimated at 0.15 s. For comparison, a lifetime at 0.01 s has been spectroscopically determined for the photoinduced state of $Na_{1.85}Co_4[Fe(CN)_6]_3{\cdot}4H_2O$.[11]

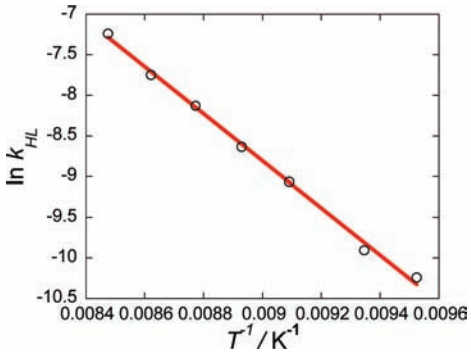

Figure 7. Arrhenius plot obtained from the parameters extracted from the relaxation curves shown in Figure 6.

In order to check the relevance of these thermodynamic parameters, we propose to reproduce the $\chi_M T$ experimental curve of the metastable RC phase.[21f] Thus, the T(TIESST) curve $\chi_M T$ vs T combines the effects of time, temperature, and cooperativity. Figure 8 shows the calculated T(TIESST) curve

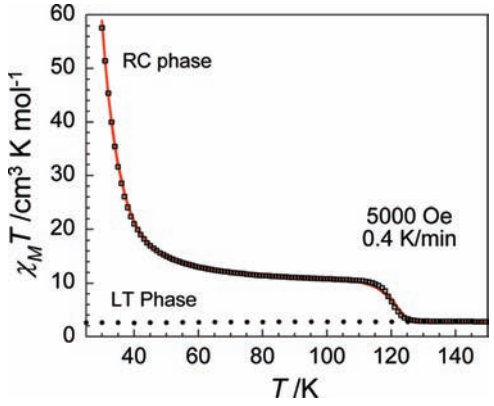

Figure 8. Thermal dependence of the $\chi_m T$ product for **1**: (●) LT phase; (□) RC phase after thermal quenching and simulation curve (red line).

(solid line) compared to the experimental curve of the RC phase (square dots). The parameters used for the simulation are the relaxation rate in the tunnelling region, $k_{HL}(T\to0)$ = 1.0 × 10^{-6} s^{-1}, the preexponential factor, $k_{HL}(T\to\infty)$ = 3.0 × 10^7 s^{-1}, the activation energy, E_a = 2010 cm^{-1}, and an additional activation energy, E_a* = 130 cm^{-1}. The agreement with these experimental data is very good. The shape and capacity of the compound to retain the trapped−induced HT information, estimated through the determination of T(TIESST), are well described. This demonstrates both the validity of our fitting procedure and our estimation of the various kinetic parameters.

CONCLUSION

In this study, we have shown that, in the 3D network $[\{Co(prm)_2\}_2\{Co(H_2O)_2\}\{W(CN)_8\}_2]{\cdot}4H_2O$, metastable states can be obtained at low temperatures either by a rapid cooling from room temperature (RC phase) or by light irradiation (PI phase). These results have been proven by powder XRD, Raman spectroscopy, optical reflectivity, and magnetometry. Kinetics, recorded from the RC phase to the LT phase, reveal a sigmoidal behavior characteristic of a cooperative system. The existence of a self-accelerated behavior is consistent with the strong cooperativity of the system, as reflected by the wide thermal hysteresis loop (225−295 K, ΔT = 70 K). We have also noticed that the metastable phases obtained by light irradiation or by thermal quenching are not strictly identical. A better comprehension allows in a future work one to perform a structural comparison between the three different PI, RC, and HT phases.

In spite of the important numbers of examples of photoswitchable compounds in the literature, very little relates the careful studies of the electronic relaxation that allows the determination of the lifetimes of the metastable states. However, knowledge of the lifetimes is crucial for future applications. Moreover, identification of the key factors that governs the lifetimes is also important to design new materials

dx.doi.org/10.1021/ic2019692 | Inorg. Chem. 2012, 51, 2852−2859

with optimized properties. From the recent studies that we have performed,[16,19,33] the lifetime of the 2D network Cs[{Co(3-cyanopyridine)$_2$}{W(CN)$_8$}]·H$_2$O has been found at 170 K at 0.14 s, very close to 0.15 s for the present Co−W 3D network. Interestingly, the geometry around the metallic centers is very similar, with Co(NC)$_4$N$_2$ and W(CN)$_8$ coordination spheres in both cases. The main difference between the two compounds, which appear to have minor consequences on the stability of the metastable state, arises from the connectivity between layers. For these two types of materials, the metastable states can be generated at low temperature by light irradiation (PI) or rapid cooling (RC). This highlights the preponderant role on intrinsic molecular factors on the relaxation processes, as the coordination spheres. A similar conclusion has been also introduced for spin-crossover compounds based on the comparison of a large variety of compounds or, more recently, by investigation of the metal dilution, which left the T(LIESST) temperature practically unchanged.[33] The preparation of new systems based on Co and W(CN)$_8$ with different coordination geometries around the Co ions is also an exciting challenge to increase the lifetimes of the metastable phase.

■ ASSOCIATED CONTENT

Supporting Information

Pictures of compound **1** in its different phases and Raman spectra recorded in the cyanide region for Cs[{Co(3-cyanopyridine)$_2$}{W(CN)$_8$}]·H$_2$O. This material is available free of charge via the Internet at http://pubs.acs.org.

■ AUTHOR INFORMATION

Corresponding Author

*E-mail: mathon@icmcb-bordeaux.cnrs.fr. Fax: +33 5 40 00 26 49.

Notes

The authors declare no competing financial interest.

■ ACKNOWLEDGMENTS

The authors thank the Aquitaine Region for supporting the photomagnetic platform and the GDRI France−Japan.

■ REFERENCES

(1) Boxhoorn, G.; Moolhuysen, J.; Coolegem, J. G. F.; Van Santen, R. A. *J. Chem. Soc., Chem. Commun.* **1985**, 1305.
(2) Miller, M. A.; Patel, M. M.; Coon, T. *Hosp. Pharm.* **2005**, *40*, 796.
(3) (a) Chapman, K. W.; Southon, P. D.; Weeks, C. L.; Kepert, C. J. *Chem. Commun.* **2005**, 3322. (b) Kaye, S. S.; Long, J. R. *J. Am. Chem. Soc.* **2005**, 6506.
(4) (a) Ferlay, S.; Mallah, T.; Ouhaes, R.; Veillet, P.; Verdaguer, M. *Nature* **1995**, *378*, 701. (b) Holmes, S.; Girolami, G. S. *J. Am. Chem. Soc.* **1999**, *121*, 5593.
(5) (a) Itaya, K.; Uchida, I.; Neff, V. D. *Acc. Chem. Res.* **1986**, *19*, 162 and references cited therein. (b) Tacconi, N. R.; Rajeshwar, K. *Chem. Mater.* **2003**, *15*, 3046−3062.
(6) Coronado, E.; Gimenez-Lopez, M. C.; Levchenko, G.; Romero, F. M.; Garcia-Baonza, V.; Milner, A.; Paz-Paternak, M. *J. Am. Chem. Soc.* **2005**, *127*, 8590.
(7) Mahfoud, T.; Molnar, G.; Bonhommeau, S.; Cobo, S.; Salmon, L.; Demont, P.; Tokoro, H.; Ohkoshi, S.-i.; Boukhedadden, K.; Bousseksou, A. *J. Am. Chem. Soc.* **2009**, *131*, 15049.
(8) Bleuzen, A.; Marvaud, V.; Mathonière, C.; Sieklucka, B.; Verdaguer, M. *Inorg. Chem.* **2009**, *48*, 3453.
(9) (a) Sato, O.; Einaga, Y.; Fujishita, A.; Hashimoto, K. *Inorg. Chem.* **1999**, *38*, 4405. (b) Bleuzen, A.; Lomenech, C.; Escax, V.; Villain, F.; Varret, F.; Cartier dit Moulin, C.; Verdaguer, M. *J. Am. Chem. Soc.* **2000**, *122*, 6648.
(10) (a) Goujon, A.; Roubeau, O.; Varret, F.; Dolbecq, A.; Bleuzen, A.; Verdaguer, M. *Eur. Phys. J. B* **14**, 115. (b) Goujon, A.; Varret, F.; Escax, V.; Bleuzen, A.; Verdaguer, M. *Polyhedron* **2001**, *20*, 1339. (c) Varret, F.; Boukheddaden, K.; Codjovi, E.; Maurin, I.; Tokoro, H.; Ohkoshi, S.; Hashimoto, K. *Polyhedron* **2005**, *24*, 2857. (d) Gawali-Salunke, S.; Varret, F.; Maurin, I.; Enaschescu, C.; Malarova, M.; Boukhedadden, K.; Codjovi, E.; Tokoro, H.; Ohkoshi, S.-i.; Hashimoto, K. *J. Phys. Chem. B* **2005**, *109*, 8251. (e) Castro, M.; Rodriguez-Velamazan, J. A.; Boukhedadden, K.; Varret, F.; Tokoro, H.; Ohkoshi, S.-i. *Eur. Phys. Lett.* **2007**, *79*, 27007.
(11) (a) Moritomo, Y.; Nakada, F.; Kamioka, H.; Hozumi, T.; Ohkoshi, S. *Phys. Rev. B* **2007**, *75*, 214110. (b) Yamauchi, Y.; Nakamura, A.; Moritomo, Y.; Hozumi, T.; Hashimoto, H.; Ohkoshi, S.-i. *Phys. Rev. B* **2005**, *72*, 214425.
(12) Cartier dit Moulin, C.; Villain, F.; Bleuzen, A.; Arrio, M.-A.; Sainctavit, P.; Lomenech, C.; Escax, V.; Baudelet, F.; Dartyge, E.; Gallet, J.-J.; Verdaguer, M. *J. Am. Chem. Soc.* **2000**, *122*, 6653.
(13) Gütlich, P., Goodwin, H. A., Eds. *Spin Crossover in Transition Metal Compounds, Topics in Current Chemistry*; Springer Verlag: Berlin, 2004; Vols. *233*−*235*.
(14) (a) Berlinguette, C. P.; Dragulescu-Andrasi, A.; Sieber, A.; Galan- Mascaros, J. R.; Güdel, H. U.; Achim, C.; Dunbar, K. R. *J. Am. Chem. Soc.* **2004**, *126*, 6222−6223. (b) Berlinguette, C. P.; Dragulescu-Andrasi, A.; Sieber, A.; Güdel, H. U.; Achim, C.; Dunbar, K. R. *J. Am. Chem. Soc.* **2005**, *127*, 6766−6779.
(15) Funck, K. E.; Prosvirin, A. V.; Mathonière, C.; Clérac, R.; Dunbar, K. *Inorg. Chem.* **2011**, *50*, 2782−2789.
(16) Li, D.; Clérac, R.; Roubeau, O.; Harté, E.; Mathonière, C.; Le Bris, R.; Holmes, S. M. *J. Am. Chem. Soc.* **2008**, *130*, 252−258.
(17) (a) Zhang, Y.; Li, D.; Clérac, R.; Kalisz, M.; Mathonière, C.; Holmes, S. M. *Angew. Chem., Int. Ed.* **2010**, *49*, 3752−3756. (b) Mercurol, J.; Li, Y.; Pardo, E.; Risset, O.; Seuleiman, M.; Rousselière, H.; Lescouëzec, R.; Julve, M. *Chem. Commun.* **2010**, *46*, 8995−8997. (c) Nihei, M.; Sekine, Y.; Suganami, N.; Nakazawa, K.; Nakao, H.; Murakami, Y.; Oshio, H. *J. Am. Chem. Soc.* **2011**, *133*, 3592−3600.
(18) Avendano, C.; Hilfiger, M.; Prosvirin, A.; Sanders, C.; Stepien, D.; Dunbar, K. *J. Am. Chem. Soc.* **2010**, *132*, 13123−13125.
(19) (a) Arimoto, Y.; Ohkoshi, S.-I.; Zhong, Z. J.; Seino, H.; Mizobe, Y.; Hashimoto, K. *J. Am. Chem. Soc.* **2003**, *125*, 9240−9241. (b) Le Bris, R.; Mathonière, C.; Létard, J.-F. *Chem. Phys. Lett.* **2006**, *426*, 380−386.
(20) (a) Ohkoshi, S.-I.; Ikeda, S.; Hozumi, T.; Kashiwagi, T.; Hashimoto, K. *J. Am. Chem. Soc.* **2006**, *128*, 5320−5321. (b) Ohkoshi, S.-I.; Hamada, Y.; Matsuda, T.; Tsunobuchi, Y.; Tokoro, H. *Chem. Mater.* **2008**, *20*, 3048−3054.
(21) (a) Létard, J.-F.; Capes, L.; Chastanet, G.; Moliner, N.; Létard, S.; Real, J. A.; Kahn, O. *Chem. Phys. Lett.* **1999**, *313*, 115−120. (b) Marcen, S.; Lecren, L.; Capes, L.; Goodwin, H. A.; Létard, J.-F. O. *Chem. Phys. Lett.* **2002**, *358*, 87−95. (c) Létard, J.-F.; Chastanet, G.; Nguyen, O.; Marcen, S.; Marchivie, M.; Guionneau, P.; Chasseau, D.; Gütlich, P. *Monatsh. Chem.* **2003**, *134*, 165−182. (d) Sanchez Costa, J.; Baldé, C.; Carbonera, C.; Denux, D.; Wattiaux, A.; Desplanches, C.; Ader, J.-P.; Gütlich, P.; Létard, J.-F. *Inorg. Chem.* **2007**, *46*, 4114−4119. (e) Létard, J.-F.; Guionneau, P.; Nguyen, O.; Costa, J. S.; Marcen, S.; Chastanet, G.; Marchivie, M.; Goux-Capes, L. *Chem.—Eur. J.* **2005**, *11*, 4582−4589. (f) Létard, J.-F. *J. Mater. Chem.* **2006**, *16*, 2550−2559.
(22) Hauser, A. *Top. Curr. Chem.* **2004**, *234*, 155 Gütlich, P., Goodwin, H. A., Eds. *Spin Crossover in Transition Metal Compounds, Topics in Current Chemistry*; Springer Verlag: Berlin, 2004.
(23) Izumi, I.; Momma, K. *Solid State Phenom.* **2007**, *130*, 15.
(24) Kahn, O. *Molecular Magnetism*; VCH: New York, 1993.
(25) (a) Létard, J.-F.; Capes, L.; Chastanet, G.; Moliner, N.; Létard, S.; Real, J. A.; Kahn, O. *Chem. Phys. Lett.* **1999**, *313*, 115−120. (b) Marcen, S.; Lecren, L.; Capes, L.; Goodwin, H. A.; Létard, J.-F. O. *Chem. Phys. Lett.* **2002**, *358*, 87−95. (c) Létard, J.-F.; Chastanet, G.; Nguyen, O.; Marcen, S.; Marchivie, M.; Guionneau, P.; Chasseau, D.;

Gütlich, P. *Monatsh. Chem.* **2003**, *134*, 165−182. (d) Sanchez Costa, J.; Baldé, C.; Carbonera, C.; Denux, D.; Wattiaux, A.; Desplanches, C.; Ader, J.-P.; Gütlich, P.; Létard, J.-F. *Inorg. Chem.* **2007**, *46*, 4114−4119. (e) Létard, J.-F.; Guionneau, P.; Nguyen, O.; Costa, J. S.; Marcen, S.; Chastanet, G.; Marchivie, M.; Goux-Capes, L. *Chem.—Eur. J.* **2005**, *11*, 4582−4589. (f) Létard, J.-F. *J. Mater. Chem.* **2006**, *16*, 2550−2559.

(26) $(\chi_M T)_{mag} = CT/(T - \theta)$, with $C = 9$ cm^3·mol^{-1}·K and $\theta = +22$ K.

(27) Varret, F., Nogues, M., Goujon, A., Drillon, M., Miller, J. S., Eds. *Magnetism: Molecules to Materials*; Wiley-VCH: Weinheim, Germany, 2001; Vol. *1*, pp 257−295.

(28) (a) Létard, J.-F.; Guionneau, P.; Rabardel, L.; Howard, J. A. K.; Goeta, A.; Chasseau, D.; Kahn, O. *Inorg. Chem.* **1998**, *37*, 4432−4441. (b) Desaix, A.; Roubeau, O.; Jeftic, J.; Haasnoot, J. G.; Boukhedadden, K.; Codjovi, E.; Linares, J.; Noguès, N.; Varret, F. *Eur. Phys. J. B* **1996**, *6*, 183−189.

(29) Maurin, I.; Chernyshov, D.; Varret, F.; Bleuzen, A.; Tokoro, H.; Hashimoto, K.; Okhoshi, S.-i. *Phys. Rev. B* **2009**, *79*, 064420.

(30) Buhks, E.; Bixon, M.; Jortner, J. *J. Am. Chem. Soc.* **1980**, *102*, 2918.

(31) Hauser, A. *Coord. Chem. Rev.* **1991**, *111*, 275.

(32) (a) Yokohama, T.; Okamoto, K.; Ohta, T.; Ohkoshi, S.-i.; Hashimoto, K. *Phys. Rev. B* **2002**, *65*, 064438. (b) Kim, J. E.; Ohishi, Y.; Moritomo, Y.; Kato, K.; Takata, M.; Ohkoshi, S.-i. *Phys. Rev. B* **2007**, *76*, 014106.

(33) Balde, C.; Desplanches, C.; Wattiaux, A.; Guionneau, P.; Gütlich, P.; Létard, J.-F. *Dalton Trans.* **2008**, 2702−2707.